KSME

Springer

Journal of Mechanical Science and Technology 34 (3) 2020

Original Article
DOI 10.1007/s12206-020-0222-4

Keywords:
· Free-surfaces
· Numerical grid
· Runner blade
· CAD reconstruction

Correspondence to:
Sergio Galván
srgalvan@umich.mx

Citation:
Delgado, G., Galván, S., Dominguez-Mota, F., García, J. C., Valencia, E. (2020). Reconstruction methodology of a Francis runner blade using numerical tools. Journal of Mechanical Science and Technology 34 (3) (2020) 1237~1247. http://doi.org/10.1007/s12206-020-0222-4

Received July 2nd, 2019
Revised December 3rd, 2019
Accepted January 17th, 2020

† Recommended by Editor Seungjae Min

Reconstruction methodology of a Francis runner blade using numerical tools

Giovanni Delgado[1], Sergio Galván[1], Francisco Dominguez-Mota[2], J. C. García[3] and Esteban Valencia[4]

[1]Faculty of Mechanical Engineering, UMSNH, Michoacán, México, [2]Faculty of Mathematical Physical Sciences, UMSNH, Michoacán, México, [3]Research Center for Applied Science and Engineering, UAEM, Morelos, México, [4]School of Mechanical Engineering, EPN, Quito, Ecuador

Abstract In a hydraulic turbine, the search of a better energy exchange with the fluid has led to designs of runner blade of geometrical shapes so complex that they are considered as free-form surfaces. Since such blade characteristics are unable to be expressed by analytic functions, its complete and realistic geometrical reconstruction requires an excessive quantity of design parameters. This study proposes a coherent and robust full 3D blade numerical reconstruction methodology in which the geometrical definition of the blade is independent of its design parameters. A quantitative and qualitative fit evaluation shows that the blade surface reconstruction needs an important quantity of discrete data along the spanwise and streamwise direction to achieve a continuous and smooth definition. The results infer that the shape characteristics of damaged and worn blades without an original CAD model could be recovered, making this methodology attractive for industrial and optimization applications.

1. Introduction

In a hydraulic turbine, the interaction between the runner blade and the surrounding fluid determines how the fluid velocity is changed and deflected, transforming it in mechanical energy. Since small changes in the blade geometry have modified the runner performance, several researchers have concentrated their main efforts in the blade parameterization during its optimization process [1-4]. Francis turbines, with 3D radial-axial blades, have so twisted shape that they are considered as free-form surfaces. This means that the surface curvature has such complex geometric characteristics that it is unable to be expressed accurately by means of one or several analytic functions [5, 6].

Recently, the design techniques to obtain the blade shape have used parametric curves and surfaces, trying to reach continuity and smoothness over such complex and free-form geometries, in Ref. [7] those techniques are divided in those that use a sectional approach and those that use surface patches. In the sectional approach, 2D sections hydrofoils are stacked along the span-wise direction. This has induced the use of the conformal mapping of the planar blade sections to cylindrical surfaces to represent the length and angle distortions of the blade [8-11]. To avoid this, in the surface method, a 2D camber surface (CS) is created and a thickness distribution (TD) is placed normally to it [12, 13]. In both methods the number and position of the TD or hydrofoil sections on a CS had to be determined arbitrarily and the pressure and suction side (PS and SS) of the blade defined by lofting or skinning the given profiles.

However, since a more detailed blade definition requires that the number of sections be increased, it continues depending on the quantity of sections used by the parametric approach. This has provoked that the number of parameters implied in the blade design also increases in an important way, which has limited its manipulation in the runner optimization [1, 4]. Thus, the major efforts must be concentrated on the search for a flexible parametric approach that can reconstruct the blade as a continuous and smooth free-form surface decoupled totally from the fluid and structural analysis and above all from the number of discrete data in order to be of

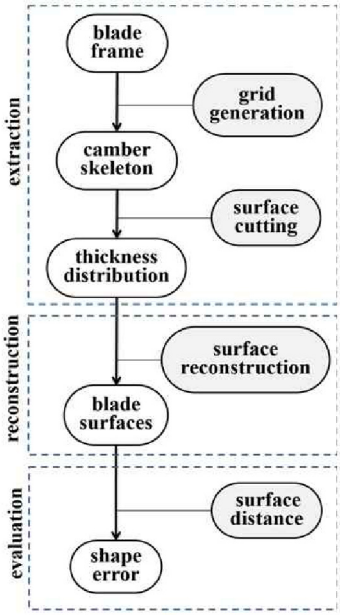

Fig. 1. Steps and algorithms used by the blade reconstruction methodology.

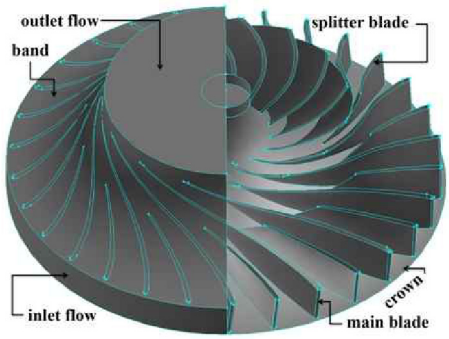

(a) Runner components

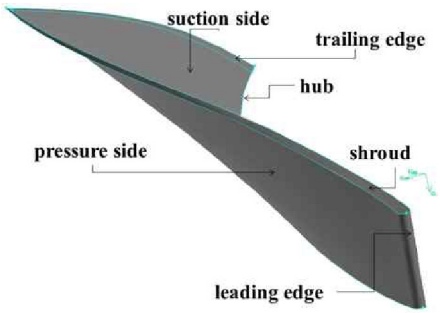

(b) Blade surfaces

Fig. 2. Components of the Francis 99 blade runner [18].

interest in design optimization purposes.

Recently, practical methodologies have used numerical grid generation to reconstruct free-form surfaces looking for a regular geometry rather than a structural performance [5, 14-16]. The grid is considered as an organized set of points formed by the intersection of the coordinate lines that are coincident with each segment of the physical boundaries and they have the same dimension as the physical region. In this context, the clustering and orthogonality of the grid lines generated by the transfinite interpolation (TFI) in the blade domain could define in a bidirectional way (spam-wise and stream-wise direction) the free-form of 3D Camber Surface as a skeleton. This multi-directional interpolation should build a grid conforming (same form or shape) to the specified boundaries of the blade. Thus, according to the grid intensity, any continuous thickness distribution data or hydrofoil section could be stacked normally to the skeleton, fitting the pressure and suction side to any prescribed tolerance to the real blade.

The tests revealed the number of stacked sections along the span-wise direction and the points along the stream-wise direction that should be needed to reach a continuous and smooth reconstructed surface. In relation to the precision in the geometrical shape characteristics reached by the analytical blade, the results infer that this reconstruction methodology could be used to recovery the original CAD models in a reverse engineering technology of the damaged or worn blades [17], preserving the design constrains imposed to the original model.

2. Methodology

The blade reconstruction methodology consists of three main steps: Extraction, reconstruction and evaluation. Several algorithms had to be designed and placed as Fig. 1 shows (in gray) to fit the numerical blade to the original one.

The first step presents how both algorithms, the grid generation and the surface cutting, were designed to extract the main features from the original blade. In the reconstruction step, the algorithm placed orthogonally to the camber-skeleton the TD on the pressure and suction sides, generating the blade surfaces. Finally, the reconstruction accuracy of the model was analyzed by a comparison between the reconstructed and real surfaces, using the surface distance algorithm.

As original blade shown in Fig. 2, we used the test-case provided by NTNU-Norwegian University of Science and Technology under the Francis 99 workshop series [18].

Fig. 2(a) presents the solids obtained from the digital file of the runner which is a structure composed of three main parts: crown, band and blades. This is a no-conventional runner since uses short blades (splitter) that alternate with long ones (main). Runner inlet and outlet flow diameters are 0.63 m and 0.349 m respectively with an inlet flow height of 0.06 m and the specific speed is 0.27. In Ref. [19] the main characteristics are explained of this kind of runners and important results are presented of its practical application.

Fig. 2(b) shows the twisted and re-flexed free-form main blade. It consists of a pressure side (PS) and a suction side (SS), and a leading edge (LE) where the water enters and a trailing edge (TE) where it exits, as well as an upper (hub) and lower (shroud) sections which are joined to the crown and band, respectively. At the blade inlet, the shroud is further forward (in the direction of the rotation) than the hub; the blade has a forward sweep.

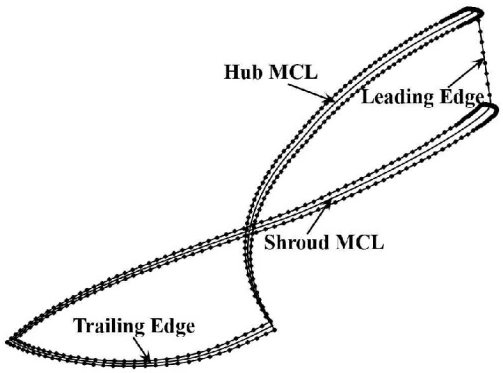

Fig. 3. Frame obtained of the real blade file.

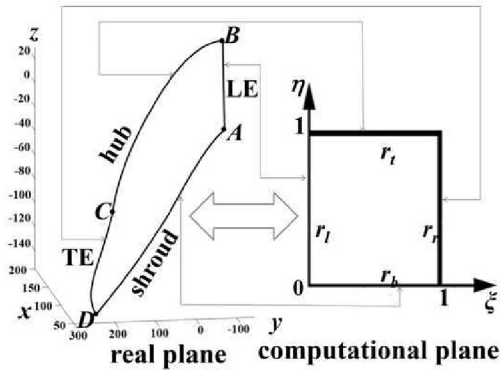

Fig. 4. Relation between the physical (mm) and computational domain.

3. Extraction of discrete data

The CAD file presented in Fig. 2(b) provides a discrete representation of the solid model with six surfaces: the pressure and suction side and the hydrofoil sections at the junction of the blades with the crown (hub) and band (shroud), and the trailing and leading sections.

To better represent the reflexed and twisted form the real hub and shroud, it was necessary to extract a considerable quantity of coordinate points from each side of the section. 106 discrete points approximated with an accuracy of three orders of magnitude the length of the well-defined pressure and suction edges.

Thus, calculating its arithmetic mean, as in Ref. [20], the mean camber line (MCL) defined the upper and lower boundaries of the numerical blade. Due to the no complex definition of the Leading and Trailing sections of the real blade, the right and left boundaries were obtained using a lesser number of points, as is shown in Fig. 3.

3.1 Grid generation algorithm

Considering the frame as the boundaries of a free-form geometry blade, the transfinite interpolation (TFI) method was used to generate the grid lines that should define the skeleton of the CS of the blade. This algebraic grid generation method [21] is based on the use of mathematical functions that interpolate among pre-assigned boundaries to generate grid lines inside the edges of the domain. In Ref. [6] the TFI to generate the mesh in the inter-blade fluid domain of an axial-radial, non-conventional runner was used. This simple and efficient algebraic method allowed controlling the clustering and orthogonality of the grid lines and, following the modeling of its boundaries, fitting the blade surfaces.

To use the TFI in our methodology, the physical domain of the real blade had to be related to a computational domain as is shown in Fig. 4. The physical plane was delimited by four 3D piecewise linear curves: The LE, the TE, the hub and the shroud, thus defining two logical directions.

The first one (ξ) starts from the leading edge r_l and ends at the trailing edge r_r, along the blade streamwise. The second direction (η) is defined by the curved line that goes from the band r_b to the crown r_t along the blade spanwise. In the computational plane r_b is the bottom edge, r_t the top edge, r_l the left edge and r_r the right edge, fulfilling the consistency conditions:

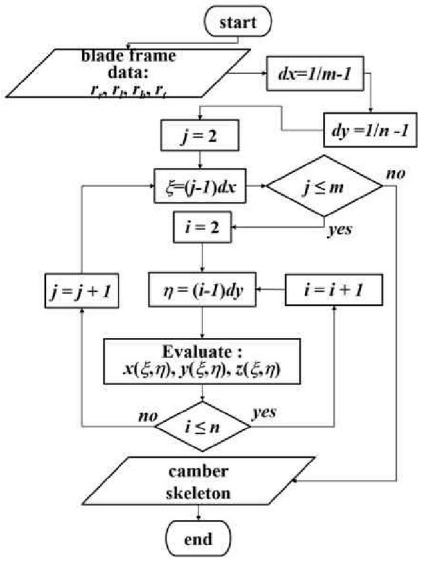

Fig. 5. Definition of the grid generation algorithm.

$$A = r_b(0) = r_l(0) \quad (1)$$

$$B = r_t(0) = r_l(1) \quad (2)$$

$$C = r_b(1) = r_r(0) \quad (3)$$

$$D = r_r(1) = r_t(1) \quad (4)$$

where A, B, C and D are the four vertices of the physical domain.

Fig. 5 presents the algorithm created to generate the grid in the computational domain. Afterwards, the algorithm returns the grid to the physical domain to erect the skeleton of the camber surface.

In Fig. 5, *m* and *n* are the number of points selected to define the TFI mesh. Eqs. (5)-(7) were used to obtain the grid points in the physical domain.

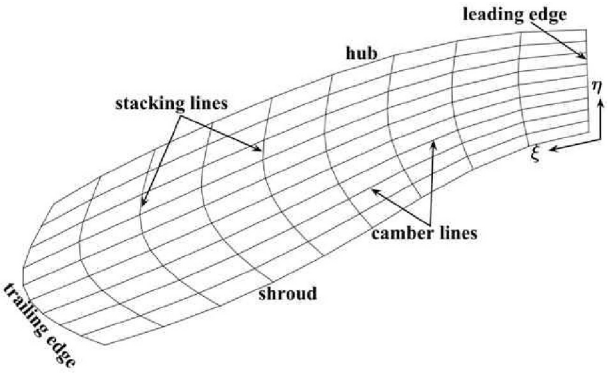

Fig. 6. Skeleton generated on the CS in the physical domain of the blade.

$$x(\xi,\eta)=(1-\xi)x_l\eta+\xi x_r(\eta)+(1-\eta)x_b(\xi)$$
$$+\eta x_t(\xi)-(1-\xi)(1-\eta)x_b(0)-(1-\xi)\eta x_t(0) \quad (5)$$
$$-(1-\eta)\xi x_b(1)-\eta\xi x_t(1)$$
$$y(\xi,\eta)=(1-\xi)y_l\eta+\xi y_r(\eta)+(1-\eta)y_b(\xi)$$
$$+\eta y_t(\xi)-(1-\xi)(1-\eta)y_b(0)-(1-\xi)\eta y_t(0) \quad (6)$$
$$-(1-\eta)\xi y_b(1)-\eta\xi y_t(1)$$
$$z(\xi,\eta)=(1-\xi)z_l\eta+\xi z_r(\eta)+(1-\eta)z_b(\xi)$$
$$+\eta z_t(\xi)-(1-\xi)(1-\eta)z_b(0)-(1-\xi)\eta z_t(0) \quad (7)$$
$$-(1-\eta)\xi z_b(1)-\eta\xi z_t(1)$$

Fig. 6 shows the camber skeleton built with the same number of grid points in each direction and uniformly spaced. The curves, where ξ is constant, corresponds to the camber lines which are used to define the flow surface. The curves, where η is constant, corresponds to the stacking lines, which can control the spanwise shape of the blade surface.

Due to the free-form shape of the blade, the camber lines and the stacking lines as main components of the camber skeleton are nearly orthogonal. The intersection of those grid lines forms now a set of data points in the real space of the blade. This structured information will help to extract important discrete data directly from the original blade.

3.2 Surface cutting algorithm

The next step of the methodology was to create a surface-surface cutting algorithm based on the orthogonal tensor product to place surfaces normal to the camber skeleton. The algorithm shown in Fig. 7 was incorporated to the methodology looking for: First, knowing precisely the real bending and thickness distribution at interior sections and second, having reference points to evaluate the fitness of the reconstructed blade.

As the Fig. 8(a) illustrates, the cutting sections were stacked orthogonally to the camber skeleton, intersecting the blade surfaces of the real blade. The intersections demarcated the PS and SS of eight hydrofoil sections along the spanwise direction. Although along the spanwise direction, each hydrofoil section has different length, 106 data points also defined pre-

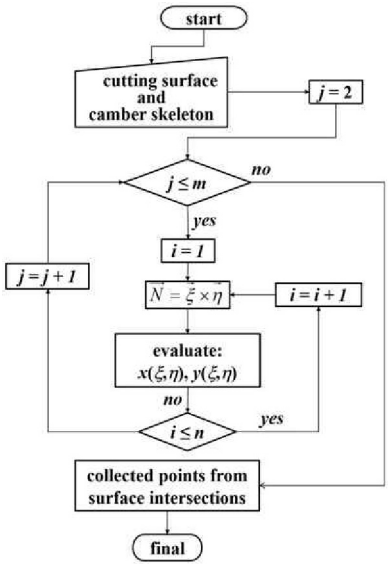

Fig. 7. Definition of the surface cutting algorithm.

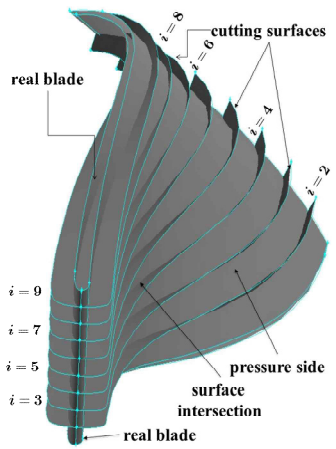

(a) Cutting surfaces along the spanwise

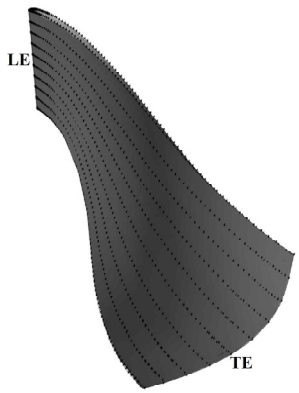

(b) Collected points on the blade surfaces

Fig. 8. Applying the surface cutting technique to the real blade.

cisely, continuously and smoothly, like the hub and shroud, each PS and SS edges of the interior sections, as shown in Fig. 8(b). Later, these same set of collected points will allow evalu-

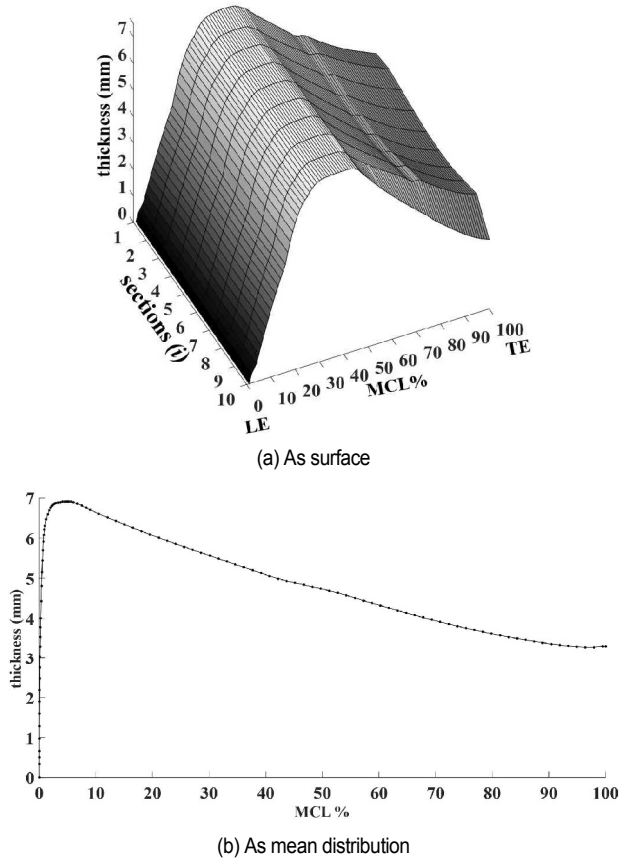

(a) As surface

(b) As mean distribution

Fig. 9. Evolution of the distribution of the hydrofoil thickness.

ating, using Eq. (8), the fitting approach reached by the numerical blade.

In Ref. [22], an algorithm to intersect the blade surfaces with horizontal cutting planes, perpendicular on the rotating axes is defined. However, when using this technique with radial-axial blades, the extracted section presented an irregular thickness distribution in relation to the one taken from the shroud and hub sections. Moreover, the number of sections with a leading a trailing edge was limited since the horizontal cutting planes intersected each edge at different levels.

3.3 Evolution of the thickness distribution

To know precisely the bending and thickness behavior of the real blade at interior sections, the collected data from each hydrofoil were related to the MCL. These data are shown as a surface in Fig. 9(a) which represents the evolution along the spanwise direction of the TD of the real blade. It is evident that the TD maintains the same evolution in the first 50 % of the mean camber line. This means the main evolution changes are presented after the maximum thickness, towards the blade TE. Therefore, this TD evolution change presents a standard deviation of 1.6 mm or 0.25 % in relation to the runner diameter.

Although in Ref. [13] it is demonstrated that not only the thickness distribution but also its evolution can modify hydrodynamic and mechanically the runner performance, to define different sections at limited span positions will implies an increase in the number of parameters involved in the reconstruction process. Instead, if we stack the mean TD in a considerable number of span positions, we would face to find compromise between quality description and parametric dimension.

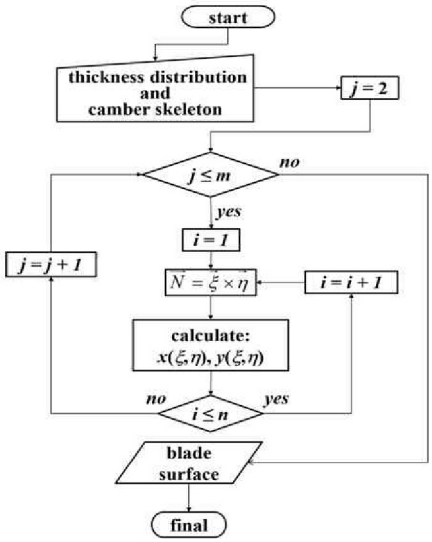

Fig. 10. Definition of the blade reconstruction algorithm.

Fig. 9(b) shows the curve build by the interpolation of 106 collected discrete points. As a result, the symmetric thickness distribution has now a continuous definition, and it can be related to the MCL percentage of the arc length section profile. This is one of the three types of thickness definition techniques presented by Ref. [7].

Since this methodology measured the thickness distribution directly on the real space, it was avoided possible distortion and discontinuity of each blade section.

4. Blade reconstruction

With the discrete values extracted from the real blade, now the reconstruction methodology is directed to achieve a continuous definition of the blade surfaces. The surface reconstruction algorithm, shown in Fig. 10 and based on the orthogonal tensor product, allowed using the camber-skeleton and the thickness distribution as input, arranging all this information in a such way that the pressure and suction side of the blade were built up as continuous and smooth surfaces.

4.1 Camber skeleton

To add more control and definition to the camber-skeleton, the algorithm presented in Fig. 5 build its mesh density through a bidirectional distribution.

Fig. 11 shows the different grid intensity determined along the spanwise (η) and streamwise (ξ) direction of the real blade. While the camber-skeleton was built, the algorithm based on

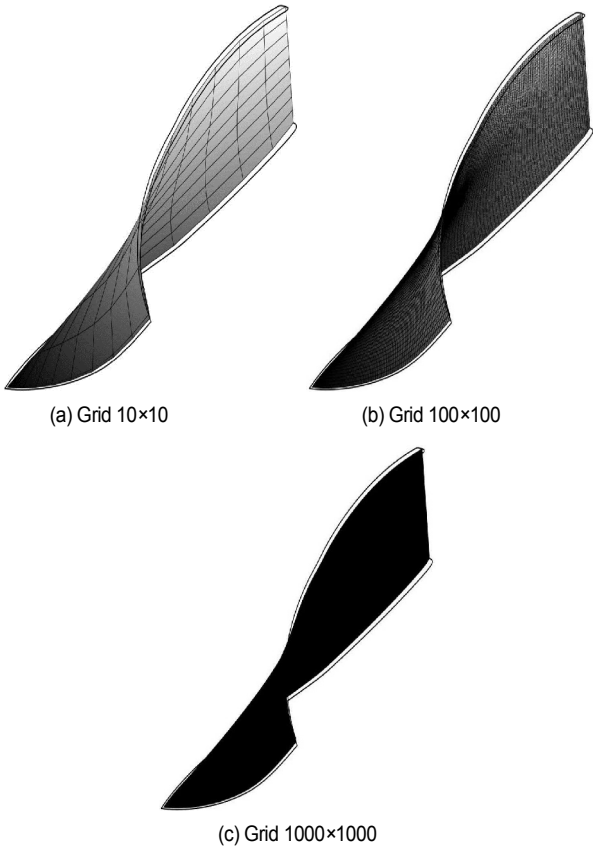

(a) Grid 10×10 (b) Grid 100×100

(c) Grid 1000×1000

Fig. 11. Definition of the skeleton inserted into the CS of the real blade.

TFI showed to be computationally efficient to conform different grids to the specified boundaries.

The camber and the stacking lines as main components of the camber skeleton are actually composed by a set of data-points. These points will serve now as real coordinates in which the TD will be placed directly in the real space of the original blade.

4.2 Hydrofoil definition

Fig. 10 shows the algorithm based on the orthogonal tensorial product which permitted that the main TD, shown in Fig. 9(b), were placed symmetric and orthogonally to the camber-skeletons, shown in Fig. 11. Besides, the TD was transposed directly on the real space using the same MCL percentage and placed normal to it as shown in Fig. 12. This procedure was focused on suppress the mapping process, used in Ref. [23], in which the conformal plane is applied to obtain the values and then they are brought back to real space. Since Fig. 9(b) presents a continuous TD along the streamwise direction, it was possible to extract the same number of discrete points that each skeleton demanded, which resulted in an advantage of this technique. Thus, a smooth and continuous hydrofoil definition was obtained at its upper and lower half-sections as the number of grid points of the skeleton was increased, Figs. 12(a)-(c).

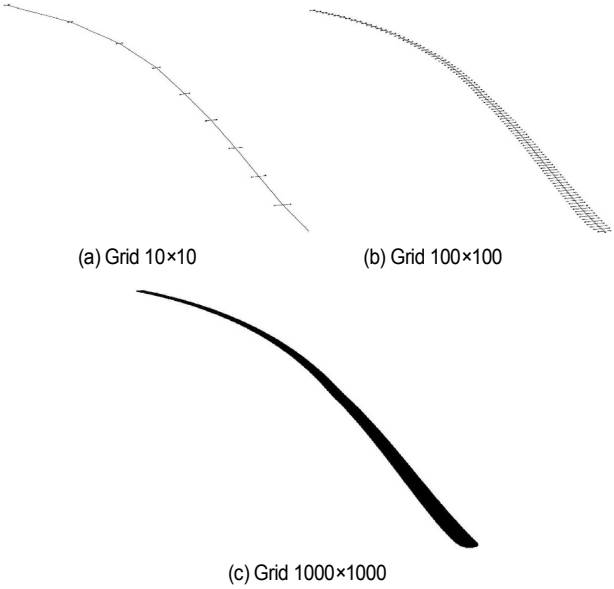

(a) Grid 10×10 (b) Grid 100×100

(c) Grid 1000×1000

Fig. 12. Definition of the blade hydrofoil.

4.3 Blade surface definition

For each camber-skeleton defined in Fig. 11, the surface reconstruction algorithm had to use the same number of grid points, $n = m$, to define the blade surfaces.

For this reason, Fig. 13(a) shows an irregular distribution of the grid points over the PS and SS when the camber-skeleton, Fig. 11(a), was only defined with ten points. This resulted in a poor resolution of the blade surface due to the different relation between streamwise and spanwise length, which is a characteristic of runners of low specific velocity.

On the contrary, when a finer camber-skeleton mesh was used, as shown in Fig. 11(b), a cloud of points was established, which makes the spanwise and streamwise evolution more continuous and not discrete, as shown in Fig. 13(b). Therefore, a more intense bidirectional control should permit a better surface definition.

When 1M of grid points was employed to define the camber-skeleton, Fig. 11(c), continuous blade surfaces were obtained, as shown in Fig. 13(c). This resulted in an enormous point quantity where the pressure and suction surfaces were continuously defined.

The methodology generated a runner blade from a cloud of points instead of surfaces patches or sectional approaches presented by Ref. [7]. This avoided the influence of not only the number of sections but also the different loft settings or skinning techniques in achieving the final shape of the blade surface.

Now, it is necessary to analyze the accuracy of the reconstructed geometry; hence, a qualitative and quantitative shape error comparison was developed.

5. Shape error evaluation

Since the objective of this work is to obtain a reconstructed

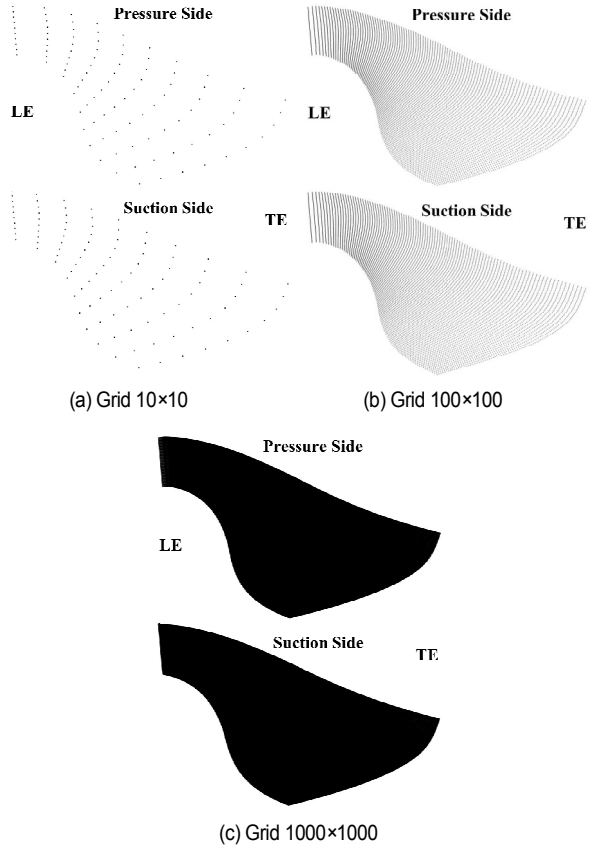

Fig. 13. Definition of the blade surfaces.

free-form blade, in this section the fit reached to the real one was evaluated carefully using Eq. (8).

$$\mathbf{d} = \frac{\left|\left(a x_i + b y_i + c z_i + d\right)\right|}{\sqrt{a^2 + b^2 + c^2}} \tag{8}$$

where **d** is the deviation between the plane created by the collected points, shown in Fig. 8(b) (*a*, *b*, *c* and *d*), and the grid points created by the orthogonal tensor product algorithm on the pressure and suction side (x_i, y_i and z_i), Fig. 13. Thus, the shape mean error is given by Eq. (9).

$$RMSE = \sqrt{\frac{\sum_{i=1}^{N} \mathbf{d}_i^{\,2}}{N}} \tag{9}$$

5.1 Quantitative approximation

Fig. 14 presents the fit reached between the analytical and the real blade as the camber-skeleton mesh was increased. Eq. (8) allowed calculating the distance between the points generated by the analytical blade and those collected from the real blade shown in Fig. 8(b). With this distance, the mean and maximum shape error presented by each approximation was calculated. In both errors there is a clear trend of decreasing, from one to five orders of magnitude, when the blade was defined using *m* = *n* = 100 and *m* = *n* = 1000 grid points. After that, the reconstruction method started to converge; the error had not an important numerical reduction. However, to know the significance of this numerical error, mainly when 100 to 1000 grid points per side, a hydrodynamic and structural study should be undertaken.

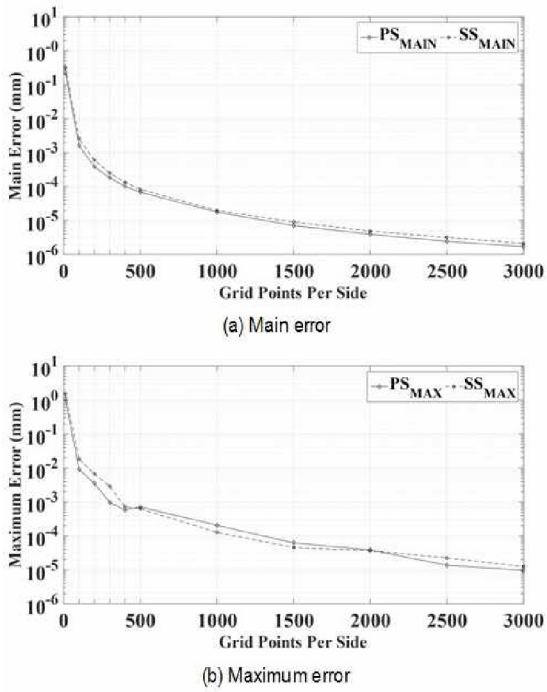

Fig. 14. Blade fit error in mm.

Previous techniques reconstructed the blade generating a surface from a set of profiles. In Ref. [9] the runner blade with five sections on a 2D meridional plane is presented. In Refs. [10, 11] a thickness distribution on three sections is used and in Ref. [24] seven previously defined sections to describe an axial blade are stacked. In Ref. [23] eleven streamlines to stack NACA hydrofoils are used. However, Fig. 14 confirms the necessity of stacking a greater number of cross-sections along the spanwise direction to better approximate the real shape of a blade.

In Ref. [25] maximum deviations of 0.044 mm in a totally axial airfoil blade are reported. Meanwhile, in Ref. [26] a final RMS error of 10.61 mm of the reconstructed surface of a real axial-radial blade is obtained. In Ref. [27] an average error of 0.004 mm as displacement of measured points from the nominal surface of an axial blade is reached.

Ref. [28] considered, in an axial-radial blade, a maximum error of 5 mm, (0.1 % of the turbine diameter) as valid to accept a blade reconstruction. Table 1 presents the maximum error, in relation to the real runner diameter, reached by this methodology. Using a grid size of 100×100, it was possible to improve by two orders of magnitude the error previously established.

Fig. 15 shows the volume change of the reconstructed blade in relation to the volume of the real blade as the grid size in-

Table 1. Maximum error, in relation to the runner diameter, between blade surfaces.

Case	Grid points	Maximum error (%)	
		Pressure side	Suction side
1	10 × 10	1.76×10^{-1}	2.49×10^{-1}
2	100 × 100	1.45×10^{-3}	2.90×10^{-3}
3	200 × 200	5.63×10^{-4}	1.07×10^{-3}
4	300 × 300	1.54×10^{-4}	4.58×10^{-4}
5	400 × 400	9.14×10^{-5}	1.14×10^{-4}
6	500 × 500	1.13×10^{-4}	9.90×10^{-5}
7	1000 × 1000	3.25×10^{-5}	2.02×10^{-5}
8	1500 × 1500	9.86×10^{-6}	7.18×10^{-6}
9	2000 × 2000	6.08×10^{-6}	5.77×10^{-6}
10	2500 × 2500	2.16×10^{-6}	3.57×10^{-6}
11	3000 × 3000	1.54×10^{-6}	1.96×10^{-6}

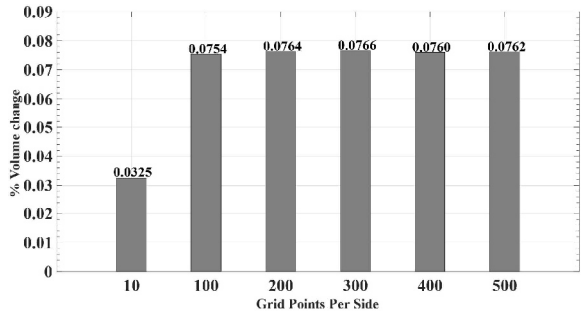

Fig. 15. Relative volume change (%) of the numerical blade.

creases. The reconstructed blade suffers a relative volume variation of 0.0754 % when a grid size of 100×100 defined the camber-skeleton. When the blade is reconstructed using a grid size greater than 100 points per side, the relative volume change remains almost constant. If we use this parameter as a predictor of a better shape definition, this no relative volume change could imply that the reconstructed blade has been totally defined and it contains now smoothing and continuous pressure and suction surfaces.

Fig. 13 showed the changes in the surfaces definition when the grid size of the CS was increased by an order of magnitude. Fig. 16 shows the rapid absolute error convergence of the relative volume change and maximum error as de number of grid size used for the reconstruction increase. We can observe that, for the volume change, the threshold is reached at 0.001 using 300 grid points per side. The maximum shape error requires a little more grid points, 500 per side, to meet the desired precision, 0.0001.

5.2 Qualitative approximation

To visualize the shape error distribution, a blade surface was generated with levels of colors. Using Eq. (8) this approximation

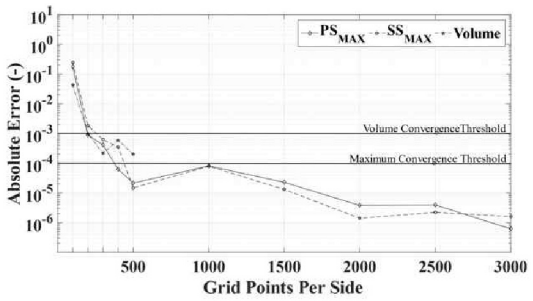

Fig. 16. Convergence history of the volume change and maximum error.

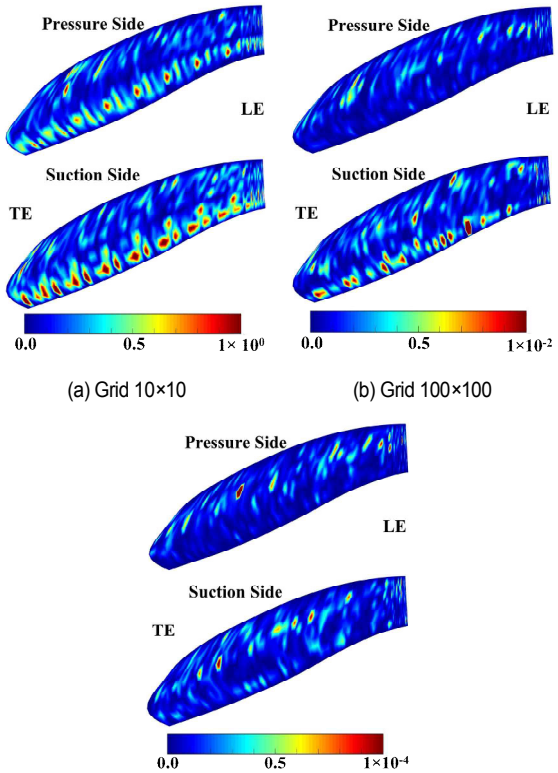

(a) Grid 10×10 (b) Grid 100×100

(c) Grid 1000×1000

Fig. 17. Shape error distribution (%) on the blade surfaces.

was assessed qualitatively and the results were transported to the pressure and suction surfaces, as shown in Fig. 17.

Fig. 17(a) illustrates the distribution of the shape differences between the analytical and the actual surfaces, when the coarser camber-skeleton was used. The maximum error reached was 1 %, and it was found all along the inferior part of the PS and SS.

Fig. 17(b) shows the shape error distribution on the blade surfaces when the grid size of the camber-skeleton was established in a finer way; one hundred points on each direction. It should be noticed that the maximum error reached in this approximation was 0.01 %, two orders of magnitude lesser than the one obtained with a mesh of ten grid points. The zones with a highest shape error were reduced in an important way. In the PS, these zones have almost disappeared. However, although

in a lower level, the difference remains along the inferior part of the SS.

Fig. 17(c) illustrates the shape error distribution on each blade surfaces when the camber-skeleton was built using one thousand points on each side. In this evaluation the error presents a maximum of 0.0001 %. The error zones along the inferior part of both sides of the blade were eliminated. However, several zones with the maximum error yet remain on the region of the highest curvature of the blade.

Previous researchers relate a better blade geometry definition with the number of the parameters involved in its design. This has limited the optimization process due to the high number of parameters that might be manipulated by the optimization algorithm. The results obtained in this work indicate that the accuracy to fit a real blade with sharp edges and high curvature variations only increases in relation to the camber-skeleton definition. Thus, the blade approximation may be independent of any blade parameterization approach used in a runner rehabilitation or upgrading process.

6. Conclusions

This work presented the numerical reconstruction of the blade geometry of a Francis runner. The design of several mathematical algorithms allowed, first, extracting discrete information from a digitalized model and then processing it to create blade surfaces of continuous and smooth shape.

Since the PS and SS were generated directly on the real blade space, this methodology eliminated problems of length distortion inherent to the twisted and reflexed axial-radial ones. Moreover, the maximum and mean deviation between the real and analytical blade were reduced only increasing the grid points used to define the blade skeleton, and no geometrical design parameters were involved.

Although a shape error convergence was unattainable, the results suggest that at least one hundred of hydrofoil sections placed along the spanwise direction would be necessary to reach an acceptable fit and no volume change. Consequently, a continuous and smooth blade could be reached, which is required at its reflexed and edges zones. However, the stacking of a standard deviation of the TD along the spanwise direction could have provoked the volume difference between the real and analytical blade.

Having tested the suitability of this methodology for reconstructing an ideal (non-defective regions within the surfaces), twisted and contortioned blade, we assume that it could be efficient to reconstruct a damaged and worn free-form blade, especially when the original surface geometry implies large data sets of unorganized points often involving measurement noise.

Consequently, the updated CAD model may be used not only to provide more realistic analysis of the part's in service performance, through CAE tools (CFD and CSM), but also to represent accurately the manufactured geometry in a Reverse Engineering process. Besides, with the simplified CAD model obtained from the Camber-Skeleton and the main TD; the blade could be parameterized considering all its design parameters at the same time rather than be focused on specific parts, which might reduce the design evaluations in an optimization process.

Acknowledgments

The authors gratefully acknowledge to the *CONACYT México*, to the *Coordinación de la Investigación Científica* of the *Universidad Michoacana de San Nicolás de Hidalgo* and to *Aulas CIMNE*, *Morelia* by the financial and technical support to accomplish this project.

Nomenclature

TFI : Transfinite interpolation
PS : Pressure side
SS : Suction side
CS : Camber surface
TD : Thickness distribution
MCL : Mean camber line
RSME : Root square mean error
CAD : Computer aided desing
CFD : Computational fluid dynamics
CSM : Computational structural mechanics
CAE : Computational aided engineering

References

[1] E. Ayli, K. Celebioglu and S. Aradag, Determination and generalization of the effects of design parameters on Francis turbine runner performance, *Engineering Applications of Computational Fluid Mechanics*, 10 (1) (2016) 545-564.

[2] S. Bahrami, C. Tribes, C. Devals, T. C. Vu and F. Guibault, Multi-fidelity shape optimization of hydraulic turbine runner blades using a multi-objective mesh adaptive direct search algorithm, *Applied Mathematical Modelling*, 40 (2) (2016) 1650-1668.

[3] A. E. Lyutov, D. V Chirkov, V. A Skorospelov, P. A. Turuk and S. G. Cherny, Coupled multipoint shape optimization of runner and draft tube of hydraulic turbines, *Journal of Fluids Engineering*, 137 (11) (2015) 111302.

[4] D. Balint, V. Câmpian, D. Nedelcu and O. Megheles, Hydrodynamics automatic optimization of runner blades for reaction hydraulic turbines, *IOP Conference Series: Earth and Environmental Science*, 15 (3) (2012) 032014.

[5] B. Gao, C. Hao, T. Li and J. Ye, Grid generation on free-form surface using guide line advancing and surface flattening method, *Advances in Engineering Software*, 110 (2017) 98-109.

[6] G. Sottas and J. D. Reymond, Mesh generation techniques for inviscid-flow simulations in turbines, *Numerical Grid Generation in Computational Field Simulation and Related Fields*, N.P. Weatherill, P.R. Eiseman, J. Hauser and J.F. Thompson (Eds.) (1994) 653.

[7] L. F. López, Surface parameterization and optimum design methodology for hydraulic turbines, *Thesis,* EPFL (2006).
[8] A. Nourbakhsh, O. S. R. H. Khodabakhsh and A. Mehrabadi, New approach for hydraulic design of Francis runner based on empirical correlations, *International Conference on Small Hydropower-Hydro Sri Lanka,* 22 (2007) 24.
[9] F. Ayancik, U. Aradag, E. Ozkaya, K. Celebioglu, O. Unver and S. Aradag, Hydroturbine runner design and manufacturing, *International Journal of Materials, Mechanics and Manufacturing*, 1 (2) (2013) 162-165.
[10] S. Thum and R. Schilling, Optimization of hydraulic machinery bladings by multilevel CFD techniques, *International Journal of Rotating Machinery*, 2005 (2) (2015) 161-167.
[11] E. Göde, Performance upgrading of hydraulic machinery with the help of CFD, *100 Volumes of 'Notes on Numerical Fluid Mechanics'*, Springer, Berlin, Heidelberg (2009) 299-310.
[12] E. Flores, L. Bornard, L. Tomas, J. Liu and M. Couston, Design of large Francis turbine using optimal methods, *IOP Conference Series: Earth and Environmental Science,* 15 (2) (2012) 022023.
[13] D. V. Chirkov, A. S. Ankudinova, A. E. Kryukov, S. G. Cherny and V. A. Skorospelov, Multi-objective shape optimization of a hydraulic turbine runner using efficiency, strength and weight criteria, *Structural and Multidisciplinary Optimization*, 58 (2) (2018) 627-640.
[14] L. Su, S. L. Zhu, N. Xiao and B. Q. Gao, An automatic grid generation approach over free-form surface for architectural design, *Journal of Central South University*, 21 (6) (2014) 2444-2453.
[15] B. Gao, T. Li, T. Ma, J. Ye, J. Becque and I. Hajirasouliha, A practical grid generation procedure for the design of free-form structures, *Computers & Structures*, 196 (2018) 292-310.
[16] Q. Wang, B. Gao, T. Li, H. Wu, J. Kan and B Hu, A triangular mesh generator over free-form surfaces for architectural design, *Automation in Construction*, 93 (2018) 280-292.
[17] C. H. She and C. C. Chang, Study of applying reverse engineering to turbine blade manufacture, *Journal of Mechanical Science and Technology*, 21 (10) (2007) 1580.
[18] C. Trivedi, M. Cervantes and O. G. Dahlhaug, *Francis 99: A Test-case on a High Head Francis Turbine*, Waterpower laboratory, Department of Energy and Process Engineering, Faculty of Engineering, NTNU-Norwegian University of Science and Technology, Trondheim, Norway (2019).
[19] M. Harano, K. Tani and S. Nomoto, Practical application of high-performance Francis-turbine runner fitted with splitter blades at ontake and shinkurobegawa No. 3 power stations of the Kansai Electric Power Co., Inc, *Hitachi Review*, 55 (3) (2006) 109.
[20] M. Banaszek and K. Tesch, Blade shape optimisation for rotor-stator interaction in Kaplan turbine, *2nd International Conference on Engineering Optimization (EngOpt2010)*, Lisboa, Portugal (2010).
[21] J. F. Thompson, B. K. Soni and N. P. Wheaterill, Transfinite interpolation (TFI) generation systems, Chapter 3, *Handbook of Grid Generation* (1998).
[22] T. Milos, A New method to obtain the blade surface intersections with horizontal cutting planes of the Francis turbine runner, *Hydraulica*, 2-3 (19) (2006) 26-35.
[23] T. Miloş and M. Bărglăzan, CAD technique used to optimize the Francis runner design, *The 6th International Conference on Hydraulic Machinery and Hydrodynamics,* Timisoara, Romania (2004) 125-130.
[24] A. Skotak and J. Obrovsky, Shape optimization of a Kaplan turbine blade, *Proceedings 23rd IAHR Symposium*, Yokohama, Japan (2006).
[25] J. Liu, J. Zhao, X. Yang, J. Liu, X Qu and X. Wang, A reconstruction algorithm for blade surface based on less measured points, *International Journal of Aerospace Engineering*, 2015 (2015).
[26] M. S. Tsuzuki, S. L. Vatanabe, E. G. Castro, E. C. N Silva, T. C. Martins, D. Taniguchi, H. S. Makiyama, A. K. Sato, G. B. Gallo, M. A. A. Garcia and H. Tiba, Development of a complete methodology to reconstruct, optimize, analyze and visualize Francis turbine runners, *IFAC-PapersOnLine*, 48 (3) (2015) 1900-1905.
[27] M. Ristic, D. Brujic and I. Ainsworth, Measurement-based updating of turbine blade CAD models: A case study, *International Journal of Computer Integrated Manufacturing*, 17 (4) (2004) 352-363.
[28] J. F. Dubé, F. Guibault, M. G. Vallet and J. Y. Trépanier, Turbine blade reconstruction and optimization using subdivision surfaces, *44th AIAA Aerospace Sciences Meeting and Exhibit* (2006) 1327.

Giovanni Delgado completed his bachelor's degree in Mechanical Engineering at the *Universidad Michoacana* in *México*. He obtained a Master of Science in Mechanical Engineering at *Universidad Michoacana* in *Mexico.* He is candidate for a Doctor of Science in Mechanical Engineering at *Universidad Michoacana in México* and Professor of the Faculty of Mechanical Engineering at the same university. His areas of interest are turbomachinery, thermofluids and numerical simulation.

Sergio Galván is a Professor and researcher of the Mechanical Engineering Faculty, *Universidad Michoacana*, *México*. He received his Ph.D in Mechanical Engineering from *L'École Polytechnique de Montréal*. As mechanical engineer, in different hydropower stations from *Comisión Federal de Electricidad*, he was responsible of the maintenance, repairing and operation of the hydraulic turbines. His main research interest includes computational design optimization applied to hydraulic turbines.

Francisco Domínguez-Mota completed a B.Sc. in Physics and Mathematics at the *Universidad Michoacana* in *México*. He obtained a Master degree in Applied Mathematics from the Center of Research in Mathematics in Guanajuato, Mexico, and a Ph.D in Mathematics at the *Universidad Nacional Autónoma de México*. He is a member of the National System of Researchers (SNI) in México, and is a researcher in Applied Mathematics at the *Universidad Michoacana*. His areas of research include numerical solution of differential equations and applications in engineering, numerical generation of structured grids and applications of optimization in large scale problems.

J. C. García is a doctor of the Centro de Ingeniería y Ciencias Aplicadas, Universidad Autónoma del Estado de Morelos, Morelos, México. He received his Ph.D in Engineering and Applied Science from Universidad Autónoma del Estado de Morelos. His research interests include turbomachinery and mechanical vibrations.

Esteban Valencia is a Professor of the Mechanical Engineering Department at the *Escuela Politécnica Nacional de Quito, Ecuador*. He received his Ph.D. in Mechanical Engineering from Cranfield University, United Kingdom. His areas of interest are turbomachinery, propulsion and fluids mechanics.